Lamella-to-Lamella Transition and Effect of Coil-Stretching on Crystallization in a Rod−Coil Diblock Copolymer Containing Poly(ϵ-caprolactone)

Xuan-Bo Liu,[†] Yong-Feng Zhao,[†] Er-Qiang Chen,*[,†] Chun Ye,[‡] Zhi-Hao Shen,[†] Xing-He Fan,*[,†] Stephen Z. D. Cheng,[‡] and Qi-Feng Zhou*[,†]

Beijing National Laboratory for Molecular Sciences, Department of Polymer Science and Engineering and Key Laboratory of Polymer Chemistry and Physics of Ministry of Education, College of Chemistry and Molecular Engineering, Peking University, Beijing 100871, China, and Maurice Morton Institute and Department of Polymer Science, The University of Akron, Akron, Ohio 44325-3909, USA

Received March 8, 2008; Revised Manuscript Received May 28, 2008

ABSTRACT: We have studied the phase properties of a diblcok copolymer poly(ϵ-caprolactone)-*block*-poly(2,5-bis[4-methoxyphenyl]oxycarbonyl)styrene) (PCL-*b*-PMPCS) with a PMPCS volume fraction of ∼59%. The mesogen-jacketed liquid crystalline (LC) PMPCS block was amorphous in the as-cast films; and would transform into a columnar (Φ) LC phase upon the first heating and thereafter serve as rod in the copolymer studied. On the basis of simultaneous measurement of small- and wide-angle X-ray scattering (SAXS and WAXS), we identified that the original microphase-separated lamellar morphology observed in the as-cast films with amorphous PMPCS block could evolve into a new lamellar morphology with a significantly increased long period. This lamella-to-lamella transition was triggered by the amorphous-to-LC transition and was irreversible. WAXS results revealed that the chain axes of the PCL block in crystal and the rod-like PMPCS block in Φ phase were all parallel to the microphase-separated lamellar normal. Since the melting temperature of PCL crystal was well below the glass transition temperature of PMPCS block, crystallization of the PCL block was taken place in one-dimensional confined environment. Compared with those confined by the amorphous PMPCS blocks, the PCL blocks were more stretched in the confinement constructed by the Φ phase of PMPCS blocks, and thus were crystallized faster with increased fold length. This work demonstrated a lamellar phase morphology evolution based on LC phase formation of the rod block, and also indicated an effect of the degree of coil stretching on polymer crystallization.

Introduction

Block copolymers (BCPs) are a fascinating class of soft matter, which can self-assemble into a variety of ordered structures with domain size ranging from a few to hundreds of nanometers.[1–3] Unlike conventional coil−coil BCPs with flexible chains as building blocks, microphase separation of rod−coil BCPs depends not only on the chain interaction, molecular weight (MW), and composition, but also on the packing behavior of the rod blocks.[4–9] Rod−coil BCP may form microphase-separated ordered lamellar phase in a much wider range of volume fraction (*f*), with various lamellar structures analogous to the liquid crystalline (LC) phases of monolayer smectic A (SmA), bilayer SmA, bilayer smectic C (SmC), etc.[4–6,10] This phase behavior is attributed to that the parallel packing of rods may overwhelm the factor of minimizing the interface area when *f* deviates far away from 0.5. On the other hand, the complex phases such as sphere and double gyroid phases, which are observed in coil−coil BCPs as the thermodynamically stable phases, can only realize in the rod−coil system with very low MW.[11]

Typical rodlike polymers incorporated in rod−coil BCPs are α-helixes such as poly(γ-benzyl-L-glutamate) (PBLG) and poly(hexyl isocyanate) (PHIC), and conjugate polymers.[5,12–14] Recently, mesogen-jacketed LC polymers (MJLCP) are also utilized as the rod blocks.[7,8,15–17] In MJLCP, the "waist" of side-chain mesogenic group is laterally attached to every second carbon atom along the backbone without a spacer or with a very short linkage.[18] Consequently, a strong steric interaction forces the backbone to extend, and the chain becomes rodlike when packed in columnar (Φ) LC phases.[19–22] The rod−coil BPCs containing MJLCP also display interesting phase behavior. For example, a bilayer "SmA" lamellar phase has been identified in a series of symmetric polystyrene-*block*-poly(2,5-bis[4-methoxyphenyl]oxycarbonyl)styrene) (PS-*b*-PMPCS) with relatively low MW.[8] Careful examination has further revealed that both low MW asymmetric and high MW symmetric PS-*b*-PMPCS may form a unique perforated layer structure with a tetragonal instead of hexagonal symmetry, where the PS chains perforate the PMPCS layers.[7] In a triblock PMPCS-*b*-PDMS-*b*-PMPCS with the majority of PMPCS, a microphase-separated cylinder phase has been recently reported.[16]

In the present work, we describe the phase properties of a diblock copolymer composed of poly(ϵ-caprolactone) and PMPCS (PCL-*b*-PMPCS, see Chart 1) with the degrees of polymerization (DP) of 200 and 98 for the PCL and PMPCS block, respectively. The phase behaviors of the sample in two

Chart 1. Chemical Structure of the PCL-*b*-PMPCS.

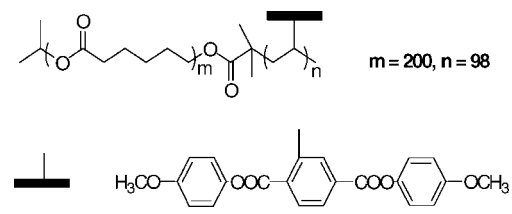

* To whom correspondence should be addressed. E-mail: (E.-Q.C.) eqchen@pku.edu.cn; (X.-H.F.) fanxh@pku.edu.cn; (Q.-F.Z.) qfzhou@pku.edu.cn.
† Beijing National Laboratory for Molecular Sciences, Department of Polymer Science and Engineering and Key Laboratory of Polymer Chemistry and Physics of Ministry of Education, College of Chemistry and Molecular Engineering, Peking University.
‡ Maurice Morton Institute and Department of Polymer Science, The University of Akron.

10.1021/ma800517k CCC: $40.75
Published on Web 06/25/2008

length scales, namely, the microphase separation and the PCL crystallization, are highly dependent on the property of PMPCS block. As reported in our pervious work of homo-PMPCS,[20] the PMPCS samples cast from solutions at below its glass transition temperature (T_g) of ~115 °C are amorphous. Upon the first heating, the homo-PMPCS with sufficiently high MW (roughly corresponding to DP ≥ ~40) develops into a Φ phase, which will be retained permanently afterward. Owing to the amorphous and Φ phases of PMPCS, the PCL-*b*-PMPCS studied also exhibited two different microphase-separated lamellar phases.

We observed an irreversible lamella-to-lamella (L−L) transition when the as-cast PCL-*b*-PMPCS was subjected to the first heating. In coil−coil BCPs or BCP solutions, the order−order transition (OOT) has been theoretically and experimentally explored.[23–30] For a thermodynamically reversible OOT, the interfacial fluctuations arises from the change of the temperature-dependent segregation power upon heating or cooling.[28] For an irreversible OOT, the initial ordered phase is usually obtained by casting a BCP solution with a solvent more selective for one block, and the morphology is then frozen due to vitrification.[26,27] When heated to above T_g, the system relaxes to the thermodynamic stable phase. In our research, the symmetry of the microphase separation was remained, but the packing of PMPCS blocks within lamellae was very different. On the basis of simultaneous measurements of small- and wide-angle X-ray scattering (SAXS and WAXS), we found that the L−L transition of the diblock was induced by the amorphous-to-LC transition of the PMPCS block.

The two lamellar phase morphologies of the PCL-*b*-PMCS in fact provided different one-dimensional (1D) confinement conditions for the PCL crystallization. Similar to other crystalline-amorphous BCPs,[31–41] the crystallization of PCL diblock largely relies on the microphase-separated structure and the property of the second block.[42,43] It has been reported that the PCL crystallization can completely overwrite the lamellar phase morphology of PCL-*b*-PB in molten state, since the crystallization temperature (T_c) is much higher than the T_g of rubbery PB.[40] For a series of PCL-*b*-P4VP with lamellar phase morphology, the high T_g P4VP layers impose a 1D hard confinement for the PCL crystallization.[38,39] Consequently, the PCL crystal orientation and growth kinetics are strongly affected by the confined size. For the PCL-*b*-PMPCS studied here, the PCL crystallization took place with hard confinement in both lamellar phase structures with different periodicities. As the amorphous-to-LC transition of PMPCS block also forces the PCL block to be further stretched, this diblock offers a unique sample to elucidate how the degree of coil stretching impacts on polymer crystallization.

Experimental Section

The PCL-*b*-PMPCS was synthesized by ring-opening polymerization of ϵ-caprolactone and subsequent atom transfer radical polymerization of MPCS.[15] The DPs of the PCL and PMPCS block of 200 and 98 were determined by ^{1}H NMR; and the diblock polydispersity of 1.14 was measured by gel permeation chromatography (GPC, Waters 2410) calibrated with polystyrene standards. The densities of the amorphous and LC PMPCS measured by a floatation technique were 1.26 and 1.28 g/cm^3 at room temperature, respectively.[20] Taking these data as approximate ones and the reported density of PCL melt,[41] we calculated that the volume fractions of PMPCS (f_{PMPCS}) were 59% and 58.6% at 80 °C for the diblock with the PMPCS in amorphous and in LC state, respectively. By using differential scanning calorimetry (DSC), the T_g of the PMPCS blocks in LC state was determined to be 110 °C, which was 5 °C higher than that of the amorphous PMPCS blocks.

The unoriented film samples were prepared by casting from a ca. 5% (w/v) chlorobenzene solution. To prevent the effect of PCL crystallization on microphase separation,[31,44] the solution was dried slowly at 80 °C. The samples were then placed in a vacuum at room temperature for a month to completely remove the residual solvent. On the other hand, to obtain oriented microphase-separated films with the PMPCS blocks staying in amorphous, we mechanically sheared the solution-cast samples at 80 °C when the samples still contained a small amount of the solvent, which could greatly reduce the viscosity. Afterward, the samples were dried in a vacuum.

1D SAXS and WAXS experiments were performed with a high-flux SAXS instrument (SAXSess, Anton Paar) equipped with Kratky block-collimation system. The scattering patterns of both SAXS and WAXS were simultaneously recorded on an imaging-plate (IP) with a pixel size of 42.3 × 42.3 μm^2 which extended to high-angle range (the q range covered by the IP was from 0.06 to 29 nm^{-1}, $q = 4\pi(\sin\theta)/\lambda$, where the λ is the wavelength of 0.1542 nm and 2θ the scattering angle). The scattering peak positions were calibrated with silicon powder for wide-angle region and silver behenate for small-angle region, respectively. After background subtraction, desmearing was performed according to the Lake's method. A temperature control unit (Anton Paar TCS300) in conjunction with the SAXSess was utilized to study the structure evolution as a function of temperature.

Two-dimensional (2D) WAXS patterns were obtained using a Bruker D8Discover diffractometer with a GADDS detector calibrated with silicon powder and silver behenate. The oriented films were mounted on the sample stage with the point-focused X-ray incident beam perpendicular to both of the shear direction (X-direction) and the shear gradient (*Z*-direction). The 2D WAXS patterns were recorded in a transmission mode at different temperatures upon heating and cooling. The background scattering was recorded and subtracted from the sample patterns.

DSC (PerkinElmer Pyris I) was used to study the crystallization and melting behavior of the PCL-*b*-PMPCS. The temperature and heat flow were calibrated with benzoic acid and indium. The samples were encapsulated in hermetically sealed aluminum pans, with a typical sample weight of approximately 2 mg. For both the samples with the PMPCS in amorphous and in LC state, nonisothermal crystallization was performed by cooling the samples from 80 °C, which is well above the melting temperature (T_m) of the PCL crystals (T_m < 65 °C for T_c < 50 °C), at a rate of 10 °C/min. Isothermal crystallization of the PCL blocks was conducted by quenching the samples at 80 °C to a preset T_c. To detect the T_m of PCL crystals formed at a T_c, the samples were directly heated to 80 at 10 °C/min after the isothermal crystallization.

Results and Discussion

The phase evolution of the PCL-*b*-PMPCS was monitored with 1D X-ray experiments at different temperatures. Parts a and b of Figure 1 show two sets of 1D WAXS patterns for the first heating and subsequent cooling of an as-cast unorientated sample, respectively. After complete removal of the solvent, the PCL blocks are crystallized at low temperatures, as evidenced by the WAXS patterns at 25 and 50 °C in Figure 1a. The peaks at q of 15.2, 15.6, and16.8 nm^{-1} can be indexed as the (110), (111), and (200) diffractions of the orthorhombic crystal lattice of PCL with a = 0.7496 nm, b = 0.4974 nm, and c = 1.7297 nm.[45] After being melted at ~60 °C, the diblock copolymer loses its molecular ordering on the subnanometer scale, and thus the high-angle diffractions disappear. On the other hand, a low-angle scattering halo at q of 3.66 nm^{-1}, which is attributed to the amorphous PMPCS blocks, is observed at below 120 °C during the first heating. When the temperature exceeds 120 °C, the low-angle scattering starts to increase in intensity; and afterward, a sharp diffraction at 4.00 nm^{-1} (i.e., a d spacing of 1.57 nm) rapidly develops. This peak has been assigned as (100) of the Φ phase formed by the PMPCS blocks.[8,20] During the first cooling, similar to that observed in the homo-PMPCS, the Φ phase diffraction gradually decreases in intensity (Figure 1b). This may be due to the fact that the

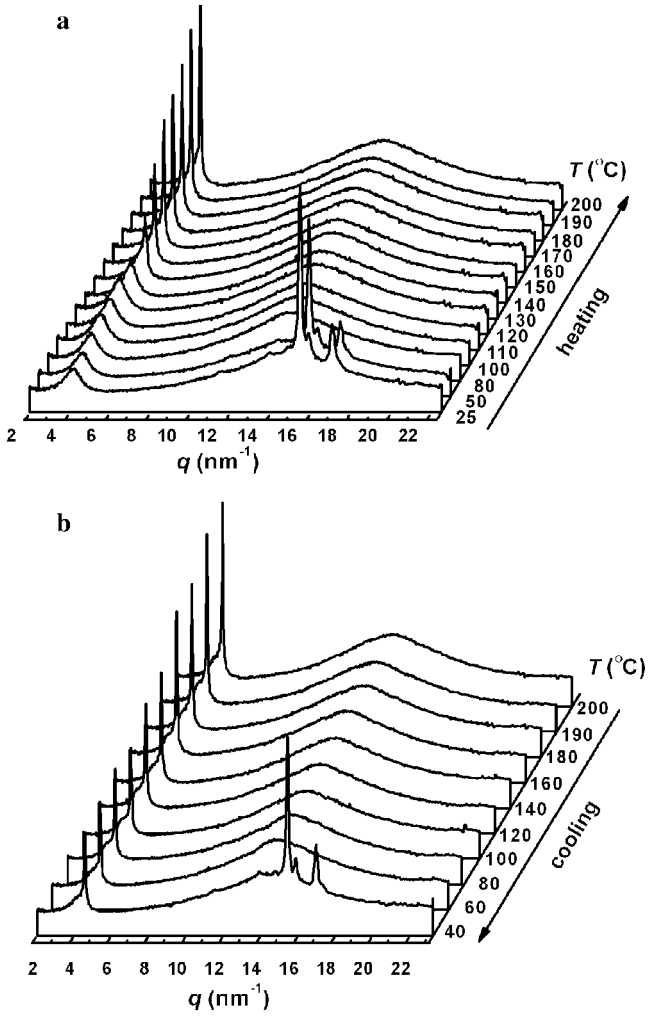

Figure 1. Sets of WAXS patterns of an unorientated PCL-*b*-PMPCS sample recorded by using SAXSess at various temperatures upon the first heating (a) and the subsequent cooling (b).

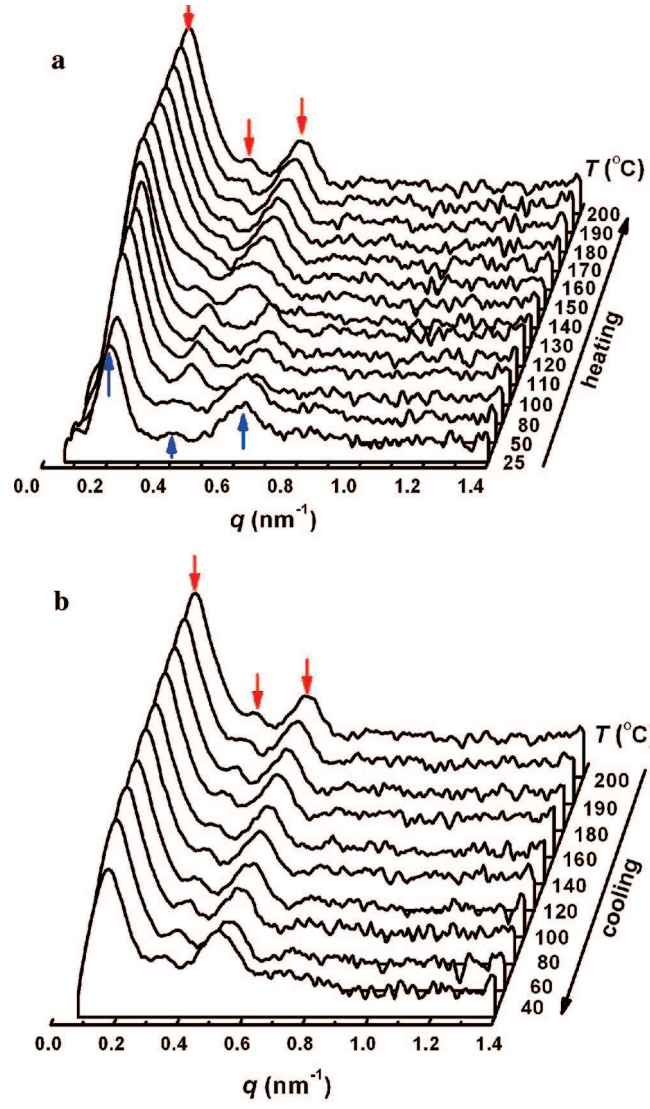

Figure 2. Sets of SAXS patterns of an unorientated PCL-*b*-PMPCS sample recorded by using SAXSess at various temperatures upon the first heating (a) and the subsequent cooling (b).

periodic electron density contrast generating the Φ phase diffraction was reduced with decreasing temperature. However, this diffraction can remain permanently after the first heating. When the sample was cooled to 40 °C, the crystallization of PCL blocks took place; the diffractions of the orthorhombic PCL crystals are restored.

Figure 2 reveals the lamellar phase morphology of the diblock copolymer with the f_{PMPCS} of 59%, where the SAXS peaks are positioned at q ratio of 1:2:3 (the peaks are indicated by arrows in Figure 2). In Figure 2a of the first heating, the sample renders the first-order scattering peaked at q of 0.21 nm^{-1} at room temperature. At below 130 °C, this scattering peak only slightly shifts toward lower q upon heating disregarding the PCL crystal melting. This means that the PCL crystal melting has little effect on the periodicity of the microphase-separated lamellae. The existence of PCL crystals within lamellae leads the electron density profile along the lamellar normal to be complicated and the form factor of PCL lamellar crystals can also affect the SAXS pattern.[38,46] This might be a reason to account for the fact that the second-order scattering is relatively weaker and broader at low temperature in comparison with that after the PCL crystal melting during the first heating. The substantial evolution of the phase morphology occurs at temperatures of 130−140 °C, wherein the first-order scattering suddenly moves to a lower q value and reaches a peak position at 0.16 nm^{-1}, indicating the occurrence of an L−L transition. Further heating the sample makes the first-order scattering gradually shift back to a q of 0.17 nm^{-1} at 200 °C. Upon the first cooling (see Figure 2b), the SAXS peaks keep essentially at the same positions disregarding the crystallization of PCL blocks at low temperature. Since the SAXS profile at 200 °C demonstrates the characteristic multiple peaks of a lamellar structure, we conclude that the order−disorder transition (ODT) temperature to the isotropic state shall be higher than 200 °C for the PCL-*b*-PMPCS, and the microphase-separated lamellar phase exists in the entire temperature range investigated.

The long periods of the microphase-separated lamellae obtained from Figures 2a and 2b are plotted as a function of temperature in Figure 3. As observed in Figures 1 and 2, the temperature at which the long period exhibits a sudden increase during the first heating is correlated with that of the Φ phase formation of PMPCS blocks. This correspondence strongly suggests that the L−L transition of microphase separation is induced by the amorphous-to-LC transition of PMPCS blocks in the lamellar layers. In Figure 1 (also see below in Figure 5, parts c and d), one may note that at the $q \sim 4.00$ nm^{-1}, the shape (100) diffraction of Φ phase always coexists with a scattering halo, which indicates that the PMPCS blocks are not fully developed into the Φ phase. However, such a LC phase formation is in fact adequate to cause the L−L transition. To form the Φ phase, the PMPCS blocks take a more extended

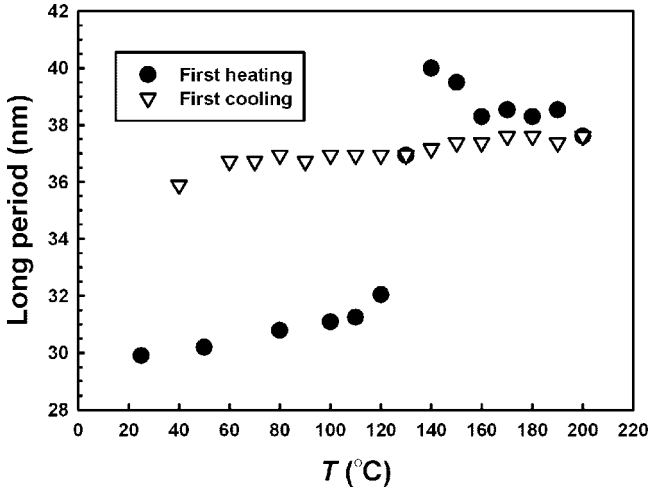

Figure 3. Long period of the PCL-*b*-PMPCS as a function of temperature upon the first heating and subsequent cooling.

conformation in comparison with the situation in amorphous state.[8,20] On the basis of the long period and the diblock composition, we estimated the PMPCS layer thickness (L_{PMPCS}) to be approximately 21.5 nm at 200 °C, which is 3.3 nm longer than that of the amorphous PMPCS layer at 80 °C. In the Φ phase at 200 °C, each repeating unite of the PMPCS block contributes 0.22 nm [=21.5 nm/(DP of 98)] to the L_{PMPCS} on average. It is noteworthy that the value of 0.22 nm/monomer agrees with the projection of one repeating unit on the chain axis of the PMPCS with rodlike conformation in the Φ phase deduced from WAXS results.[20] This indicates that the PMPCS block is extended with the chain axis oriented along the lamellar normal (also see below), and the microphase-separated lamellar structure resembles a monolayer supramolecular "SmA" phase. During the L−L transition, we observed that the long period reached a maximum of ∼40 nm at 140 °C, and the second-order scattering was smeared (see Figure 2a). This might be due to that when the PMPCS blocks started to extend from the isotropic state, the original lamellae were partially destroyed or became undulated to a certain extent. Afterward, accompanying by the substantial development of the PMPCS Φ phase, the lamellar structure relaxed toward equilibrium with a reduced long period.

The L−L transition reported here is irreversible. PMPCS can be easily dissolved in many common solvents such as THF, chloroform, toluene, chlorobenzene, *etc*. After solution casting, the resultant films are usually amorphous. This implies that even if the PMPCS chains adopt a rather extended conformation in solution, parallel packing of rodlike chains in the Φ phase cannot be directly achieved upon solvent evaporation. However, heating the as-cast PMPCS films to above T_g can irreversibly result in the thermodynamically more stable Φ phase. Therefore, for the diblock studied, the microphase-separated lamellar phase with amorphous PMPCS obtained from solution casting is at most a metastable state. In this context, although the symmetry of lamellar morphology is remained, the L−L transition we encountered here is more or less similar to the irreversible OOTs with the initial phase morphology kinetically trapped in the as-cast film due to vitrification of one phase.[26,27] Nevertheless, unlike the irreversible OOT of coil−coil block copolymers which is simply dependent on the accelerated relaxation of blocks at temperatures above T_g, the L−L transition of PCL-*b*-PMPCS involves the introduction of a new packing order on the molecular scale in the Φ phase. This L−L transition can hardly be detected upon annealing at 120 °C (<T_g of PMPCS) with a prolonged isothermal time (e.g., ∼40 h). Only with the Φ phase development can the L−L transition occur in a rather

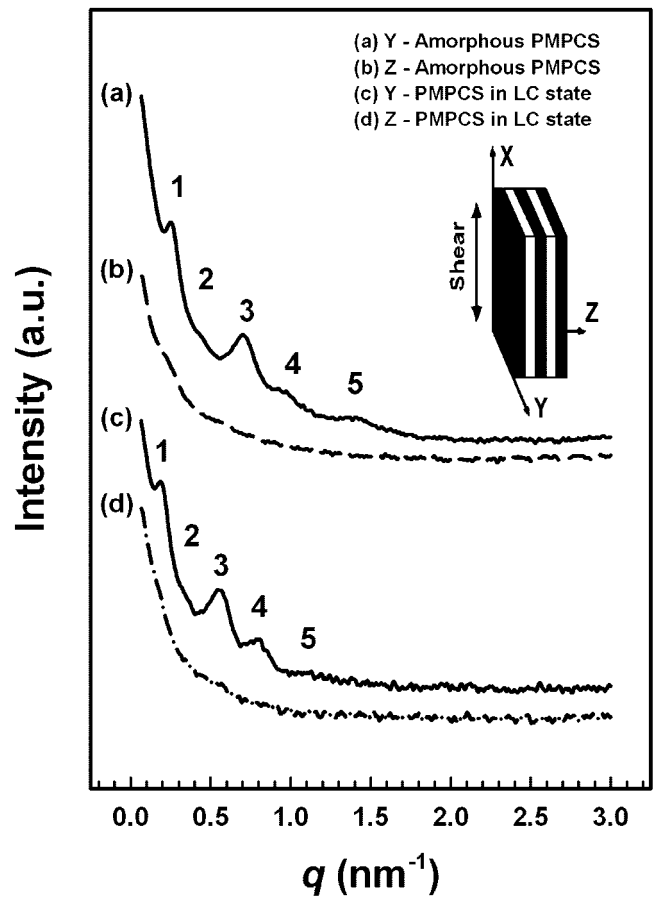

Figure 4. Smeared SAXS profiles of the sheared film recorded with the line-focused X-ray incident beam aligned parallel to *Y*- (curves a and c) and *Z*-directions (curves b and d). The inset schematically shows the film sample with the *X*- and *Z*-directions of the shear direction and shear gradient.

short time (<10 min). Therefore, the amorphous-to-LC transition of the PMPCS blocks triggers the L−L transition.

We further carried out 2D WAXS experiments to examine the chain orientations of PCL and PMPCS block with respect to the microphase-separated lamellar normal. The mechanical shear was applied for macroscopically oriented samples. Figure 4 presents 1D SAXS results for the sheared samples with the amorphous and Φ phase PMPCS blocks. The inset of Figure 4 indexes the film sample orientation. Since the desmearing program based on the Lake's method is not suitable for the orientated samples, the SAXS profiles in Figure 4 are smeared. With the line-focused X-ray incident beam perpendicular to both the shear direction (*X*-direction) and shear gradient (*Z*-direction) (i.e., parallel to the *Y*-direction), the SAXS profile gives the peaks positioned at q values with a ratio of 1:2:3:4:5 for the film sample with amorphous PMPCS blocks before the first heating (curve a in Figure 4). After the film sample was annealed at 180 °C, while the peaks move to lower q values due to the increased long period, the characteristic SAXS profile of lamellar morphology remains (curve c). However, only featureless SAXS profiles with monotonic decrease in intensity can be observed when X-ray is parallel to the *Z*-direction (curves b and d). Although without desmearing, the SAXS results recorded with the two view directions are adequate to support that the mechanical shear has resulted in parallel lamellae with lamellar normal preferentially along the *Z*-direction.[47–49]

Figure 5 collects a set of 2D WAXS patterns of a sheared film at various temperatures upon the first heating and subsequent cooling. The point-focused X-ray beam was directed

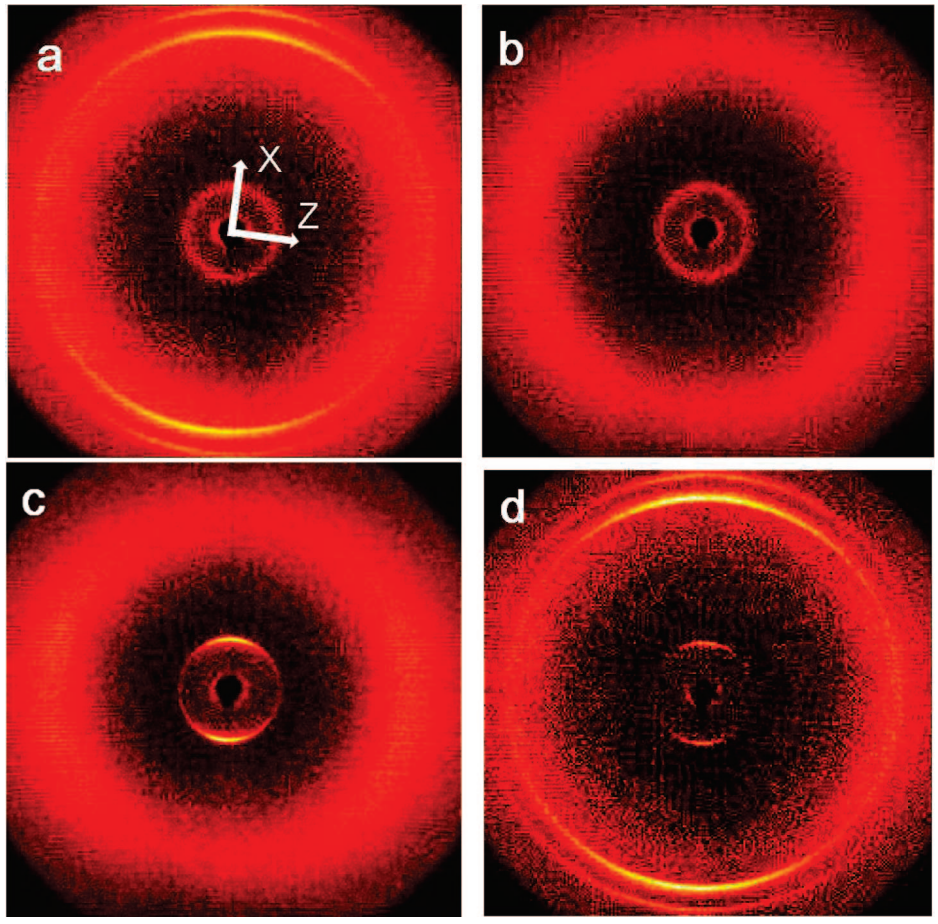

Figure 5. 2D WAXS patterns of a sheared PCL-*b*-PMPCS film with the X-ray incident beam perpendicular to the X- and Z-direction. The patterns were recorded during the first heating and subsequent cooling at (a) 25, (b) 80, (c) 160, and (d) 36 °C, respectively.

parallel to the *Y*-direction of the film. The *X*- and *Z*-directions of the film sample are indexed in Figure 5a. Before the formation of Φ phase, there is only a ring pattern at low-angle region as shown in Figure 5a at 25 °C and Figure 5b at 80 °C, evidencing the amorphous nature of PMPCS blocks within the lamellae. However, the PCL crystals render an anisotropic diffraction pattern in the high-angle region (Figure 5a). Despite the relatively broad azimuthal distribution, the intensity maximums of the (110) and (200) diffraction locate on X-direction, and therefore the crystallographic *c*-axis, *i.e.*, the PCL chain direction is preferentially parallel to the lamellar normal (Z-direction). This result is coincident with the observation in PCL-*b*-P4VP diblock copolymers with the PCL layer thickness greater than 8 nm.[38,39] Melting of the PCL crystals results in the isotropic scattering in high-angle region (Figure 5b). At 160 °C, a pair of sharp low-angle diffractions with the *d* spacing of 1.57 nm displays on X-direction (Figure 5c), which is attributed to the interference between the rodlike chains with the diffraction direction perpendicular to the columnar axis of Φ phase. Note that the microphase-separated lamellar orientation is kept after the Φ phase formation (see Figure 4). Figure 5c in fact reveals that the PMPCS rod axis is also parallel to the lamellar normal.[8] Such an orientation of the PMPCS remains during the subsequent cooling. After the PCL was crystallized (Figure 5d), the (110) and (200) diffractions reappear, with the azimuthal distributions essentially same to that in Figure 5a. As a result, the PCL and PMPCS blocks share the same chain orientation.

It is interesting to ask how the Φ phase formation of PMPCS blocks influences the crystallization of PCL blocks. Note that both the T_gs of the amorphous and LC PMPCS are higher than 100 °C, which are well above the T_m of PCL. Consequently, the PCL crystallization is always subjected to a 1D hard-confined nanoenvironment. We found that the PCL crystallization at different T_cs hardly altered the SAXS patterns of the diblock, confirming that the lamellar morphology was essentially preserved due to the hard confinement condition.[32,34,38] As shown in Figures 2 and 3, the long period of PCL-*b*-PMPCS increases significantly after the L−L transition. Since the f_{PMPCS} difference between the samples with PMPCS in amorphous and in LC state is trivial, this observation also reflects that the PCL layer thickness (L_{PCL}), and thus the dimension of the PCL coils along the lamellar normal, gains a considerable increment. The values of L_{PCL} at 80 °C were estimated to be nearly 12.6 and 15.2 nm for the sample before and after the first heating, respectively. The comparison between the two L_{PCL} values gives that after the L−L transition the molten PCL blocks are 20% more elongated. We consider that while the PMPCS blocks extend to be rodlike, the average interfacial area occupied by a single chemical junction point decreases and thus causes the further stretching of PCL blocks.

With a higher degree of stretching, the PCL blocks demonstrated an accelerated crystallization process, which was readily observed *via* nonisothermal crystallization experiments. Upon cooling at a rate of 10 °C/min from 80 °C where the PCL crystals were completely melted, the nonisothermal crystallization of the sample with the PMPCS in Φ phase was initiated at 27.6 °C, 5.4 °C higher than that observed when the PMPCS was amorphous. We further studied the isothermal crystallization kinetics of the samples before and after the Φ phase formation. The exothermic processes of the PCL isothermal crystallization were recorded by DSC. The peak time (t_{peak}) of the exotherm was taken as the indication of overall crystallization rate, and

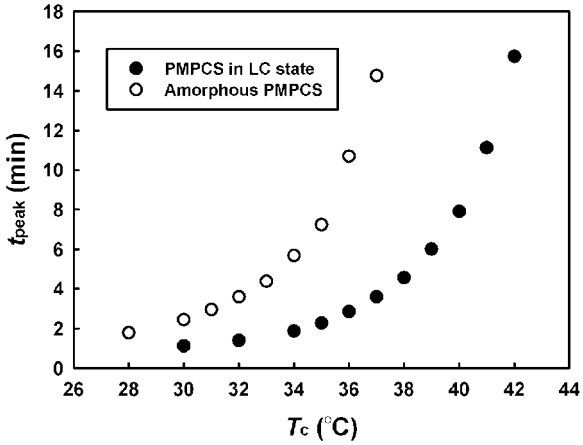

Figure 6. Plot of t_{peak} of the exotherm of isothermal crystallization as a function of T_c. Key: (○) sample with amorphous PMPCS; (•) sample with PMPCS in the LC state.

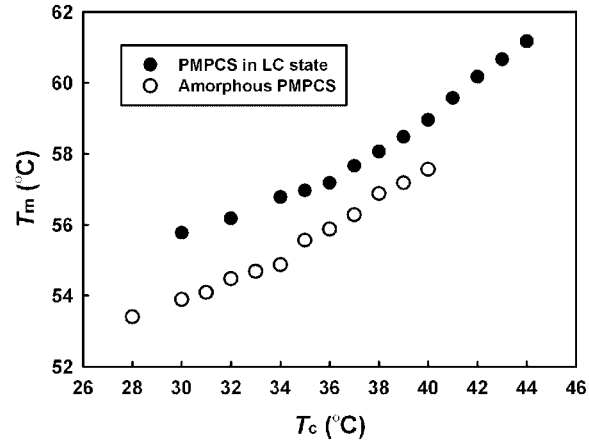

Figure 7. Plot of T_m of the PCL crystals formed in isothermal crystallization as functions of T_c. Key: (○) sample with amorphous PMPCS; (•) sample with PMPCS in LC state.

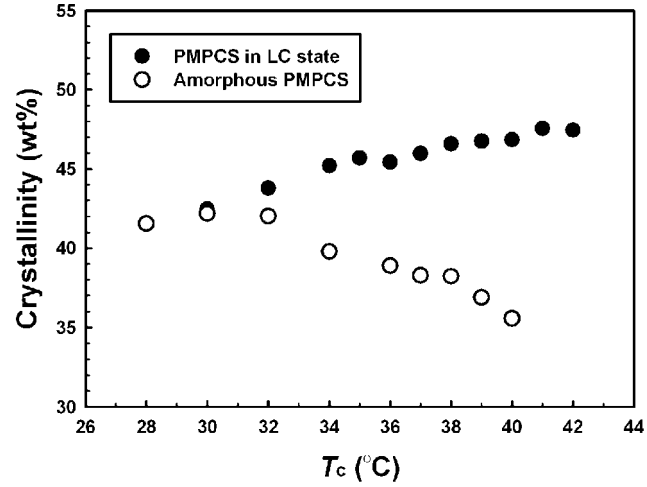

Figure 8. Plot of crystallinity (X_c) of the PCL crystals formed in isothermal crystallization as functions of T_c. Key (○) sample with amorphous PMPCS; (•) sample with PMPCS in LC state.

the results are summarized in Figure 6. Obviously, at a same T_c, the t_{peak} of the sample with rodlike PMPCS is always shorter, i.e., the crystallization is faster, than that of the sample with amorphous PMPCS.

Using the DSC curves, we further carried out the Avrami analysis based on the equation of $X_c(t) = 1 - \exp(-Kt^n)$, where $X_c(t)$ is the normalized degree of crystallinity that has formed at time t, K the prefactor, and n the Avrami exponent. We found that for both different lamellar phases, the values of n deduced from the double logarithmic plot of $\log[-\ln(1 - X_c(t))]$ vs $\log t$ were all around 1.9. Since the crystallization occurred within the thin layers of PCL, the n close to 2 may refer to a 2D athermal nucleation mechanism.[50] Consequently, we presume that the PCL crystallization starts from the heterogeneous nucleation, despite the two different lamellar phase morphologies.[35,38] However, the PCL crystal growth thereafter shall be affected by the size of 1D confined space. We speculate that within the layers with a larger L_{PCL}, the adjustment of the coil to the conformation suitable for packing in the crystal lattice may become easier. More importantly, the more elongated PCL coils may provide a certain degree of preorder in comparison with that of the sample with amorphous PMPCS, and this leads to a faster crystal growth. Figure 6 shows that the difference in t_{peak} for the samples with amorphous and with LC PMPCS enlarges with increasing T_c. As the surface nucleation barrier of crystal growth is strongly temperature-dependent, we consider that the stretching of the PCL blocks mainly helps the crystallization overcome the surface nucleation barrier.

We also examined the melting behavior of the PCL crystals confined in the two different microphase-separated lamellar phases. In both cases, the T_m of PCL crystals monotonically increases with increasing T_c as shown in Figure 7. However, compared with that of the PCL crystals grown within the thinner PCL layer between two adjacent amorphous PMPCS layers, the T_m of PCL formed in the confinement of the LC layers at the same T_c is 1−2 °C higher. One possible reason to account for the increase of T_m is that the entropy of the more stretched PCL blocks in molten state is decreased.[50] Moreover, similar to that usually observed in polymer crystallization, a higher T_m of lamellar crystals may reflect a larger fold length. For the PCL-*b*-PMPCS we studied, the larger L_{PCL} may facilitate the growth of thicker PCL lamellar crystals. Therefore, the result shown in Figure 7 also indicates that the PCL lamellar thickness is dependent not only on the supercooling but also on the degree of coil stretching.

Figure 8 depicts the crystallinity X_c, which was measured after prolonged isothermal time, as functions of T_c. It is intriguing to find that with increasing T_c, the X_c of the sample with amorphous PMCPS slightly decreases, whereas in the thicker PCL layers the X_c of the sample with LC PMPCS gradually increases. Parts a and d of Figure 5 demonstrate that the azimuthal distributions of the (110) and (200) diffraction of the PCL formed in two different confinement conditions are essentially the same. This means that the PCL crystals in both lamellar phase morphologies share the same orientation, which may be possibly ascribed to that the PCL crystallizations are initiated by the same heterogeneous nucleation. Within the 1D hard confinement, the lateral growth of the PCL lamellar crystals will stop when the neighboring crystals impinge with each other. At T_c below 32 °C, the PCL fold length may be considerably shorter than the L_{PCL} disregarding the confinement is imposed by the amorphous or LC PMPCS layers. Consequently, isothermal crystallization of the PCL in both of the lamellar morphologies results in the same X_c. For the X_c decrease with increasing T_c observed in the crystallization of the diblock with amorphous PMPCS, no full explanation is available at this moment. Possibly, the spaces interlocked by the impinged PCL crystals with different chain orientations, where the crystallization is hard to take place during the isothermal condition, becomes larger when the PCL fold length is increased with T_c. However, such a confinement effect may be partially relieved when the L_{PCL} is increased after the PMPCS blocks developed into Φ phase. As the PCL *c*-axis is preferentially oriented along

the microphase-separated lamellar normal, the larger L_{PCL} allows the crystals to grow with larger fold length, particularly when the PCL blocks are more stretched. As a result, more PCL segments can be packed into the crystals, and the X_c increases accordingly.

Summary

In summary, we have investigated the phase properties of a diblcok copolymer containing the blocks of PCL and mesogen-jacketed LC polymer of PMPCS (PCL-*b*-PMPCS) with the f_{PMPCS} of ~59%. The microphase-separated lamellar structure was identified upon thermal SAXS experiments in the entire temperature range studied. The PMPCS blocks in the as-cast films stayed in the amorphous state, which transformed into a thermodynamically more stable state of Φ phase during the first heating to above 120 °C. On the basis of the simultaneous measurements of WAXS and SAXS, we concluded that the amorphous-to-LC transition of the PMPCS induced an irreversible L−L transition of the phase morphology, resulting in a significant increase in the lamellar long period. Both the chain axes of the PCL in crystals and the rodlike PMPCS in Φ phase were parallel to the normal of microphase-separated lamellae. For both lamellar phase morphologies, the PCL crystallization was subjected to a 1D hard confinement condition. As the PCL blocks were more stretched after the L−L transition, the PCL crystals with larger fold length would grow at an accelerated crystallization rate. This work demonstrated an LC formation triggered phase morphology evolution of diblock copolymer and the effect of degree of coil stretching on 1D confinement crystallization. The phase behavior of PCL-*b*-PMPCS diblock copolymers with various compositions are currently under investigation in our laboratory.

Acknowledgment. This work was supported by the National Nature Science Foundation of China (NNSFC Grants: 20234020, 20774006, 20634010, 20574002, and 50573001). We thank Prof. G. Strobl at Albert-Ludwigs-Universität Freiburg for his helpful discussion.

References and Notes

(1) Hamley, I. W. *The Physics of Block Copolymers*; Oxford University Press: Oxford, U.K., 1998.
(2) Bates, F. S.; Fredrickson, G. H. *Physics Today* **1999**, *52*, 32–38.
(3) Loge, T. P.; Muthukumar, M. *J. Phys. Chem.* **1996**, *100*, 13275–13292.
(4) Halperin, A. *Macromolecules* **1990**, *23*, 2724–2731.
(5) Chen, J. T.; Thomas, E. L.; Ober, C. K.; Mao, G. P. *Science* **1996**, *273*, 343–346.
(6) Olsen, B. D.; Segalman, R. A. *Macromolecules* **2005**, *38*, 10127–10137.
(7) Tenneti, K. K.; Chen, X. F.; Li, C. Y.; Tu, Y. F.; Wan, X. H.; Zhou, Q. F.; Sics, I.; Hsiao, B. S. *J. Am. Chem. Soc.* **2005**, *127*, 15481–15490.
(8) Li, C. Y.; Tenneti, K. K.; Zhang, D.; Zhang, H. L.; Wan, X. H.; Chen, E. Q.; Zhou, Q. F.; Carlos, A. O.; Igos, S.; Hsiao, B. S. *Macromolecules* **2004**, *37*, 2854–2860.
(9) Chen, J. Z.; Zhang, C. X.; Sun, Z. Y.; An, L. J.; Tong, Z. *J. Chem. Phys.* **2007**, *127*, 024105.
(10) Matsen, M. W.; Barrett, C. *J. Chem. Phys.* **1998**, *109*, 4108–4118.
(11) Lee, M.; Cho, B. K.; Zin, W. C. *Chem. Rev.* **2001**, *101*, 3869–3892.
(12) Gallot, B. *Prog. Polym. Sci.* **1996**, *21*, 1035–1088.
(13) Klok, H. A.; Langenwalter, J. F.; Lecommandoux, S. *Macromolecules* **2000**, *33*, 7819–7826.
(14) Klok, H. A.; Lecommandoux, S. *Adv. Mater.* **2001**, *13*, 1217–1229.
(15) Zhao, Y. F.; Fan, X. H.; Chen, X. F.; Wan, X. H.; Zhou, Q. F. *Polymer* **2005**, *46*, 5396–5405.
(16) Gao, L. C.; Pan, Q. W.; Chen, X. F.; Fan, X. H.; Zhang, X. l.; Shen, Z. H.; Zhou, Q. F *Macromolecules* **2007**, *40*, 9205–9207.
(17) Gopalan, P.; Ober, C. K. *Macromolecules* **2001**, *34*, 5120–5124.
(18) Zhou, Q. F.; Zhu, X. L.; Wen, Z. Q. *Macromolecules* **1989**, *22*, 491–493.
(19) Tu, H. L.; Wan, X. H.; Liu, Y. X.; Chen, X. F.; Zhang, D.; Zhou, Q. F.; Shen, Z. H.; Ge, J. J.; Jin, S.; Cheng, S. Z. D. *Macromolecules* **2000**, *33*, 6315–6320.
(20) Ye, C.; Zhang, H. L.; Huang, Y.; Chen, E. Q.; Lu, Y. L.; Shen, D. Y.; Wan, X. H.; Shen, Z. H.; Cheng, S. Z. D.; Zhou, Q. F. *Macromolecules* **2004**, *37*, 7188–7196.
(21) Zhao, Y. F.; Fan, X. H.; Wan, X. H.; Chen, X. F.; Yi, Y.; Wang, L. S.; Dong, X.; Zhou, Q. F. *Macromolecules* **2006**, *39*, 948–956.
(22) Zhang, H.; Yu, Z.; Wan, X.; Zhou, Q. F.; Woo, E. M. *Polymer* **2002**, *43*, 2357–2361.
(23) Laradji, M.; Shi, A. C.; Desai, R. C.; Noolandi, J. *Phys. Rev. Lett.* **1997**, *78*, 2577–2580.
(24) Laradji, M.; Shi, A. C.; Noolandi, J.; Desai, R. C. *Macromolecules* **1997**, *30*, 3242–3255.
(25) Qi, S. Y.; Wang, Z. G. *Polymer* **1998**, *39*, 4639–4648.
(26) Sakurai, S.; Momii, T.; Taie, K.; Shibayama, M.; Nomura, S.; Hashimoto, T. *Macromolecules* **1993**, *26*, 485–491.
(27) Jeong, U.; Lee, H. H.; Yang, H.; Kim, J. K.; Okamoto, S.; Aida, S.; Sakurai, S. *Macromolecules* **2003**, *36*, 1685–1693.
(28) Hajduk, D. A.; Gruner, S. M.; Rangarajan, P.; Register, R. A.; Fetters, L. J.; Honeker, C.; Albalak, R. J.; Thomas, E. L. *Macromolecules* **1994**, *27*, 490–501.
(29) Ryu, C. Y.; Lodge, T. P. *Macromolecules* **1999**, *32*, 7190–7201.
(30) Abbas, S.; Li, Z. B.; Hassan, H.; Lodge, T. P. *Macromolecules* **2007**, *40*, 4048–4052.
(31) Zhu, L.; Chen, Y.; Zhang, A.; Calhoun, B. H.; Chun, M.; Quirk, R. P.; Cheng, S. Z. D.; Hsiao, B. S.; Yeh, F.; Hashimoto, T. *Phys. Rev. B.* **1999**, *60*, 10022–10031.
(32) Zhu, L.; Cheng, S. Z. D.; Calhoun, B. H.; Ge, Q.; Quirk, R. P.; Thomas, E. L.; Hsiao, B. S.; Yeh, F.; Lotz, B. *J. Am. Chem. Soc.* **2000**, *122*, 5957–5967.
(33) Zhu, L.; Cheng, S. Z. D.; Calhoun, B. H.; Ge, Q.; Quirk, R. P.; Thomas, E. L.; Hsiao, B. S.; Yeh, F.; Lotz, B. *Polymer* **2001**, *42*, 5829–5839.
(34) Huang, P.; Zhu, L.; Guo, Y.; Ge, Q.; Jing, A. J.; Chen, W. Y.; Quirk, R. P.; Cheng, S. Z. D.; Thomas, E. L.; Lotz, B.; Hsiao, B. S.; Orta, C. A. A.; Sics, I. *Macromolecules* **2004**, *37*, 3689–3698.
(35) Sun, L.; Zhu, L.; Ge, Q.; Quirk, R. P.; Xue, C.; Cheng, S. Z. D.; Hsiao, B. S.; Avila-Orta, C. A.; Sics, I.; Cantino, M. E. *Polymer* **2004**, *45*, 2931–2939.
(36) Loo, Y. L.; Register, R. A.; Ryan, A. J.; Dee, G. T. *Macromolecules* **2001**, *34*, 8968–8977.
(37) Loo, Y. L.; Register, R. A.; Ryan, A. J. *Macromolecules* **2002**, *35*, 2365.
(38) Sun, Y. S.; Chung, T. M.; Li, Y. J.; Ho, R. M.; Ko, B. T.; Jeng, U. S.; Lotz, B. *Macromolecules* **2006**, *39*, 5782–5788.
(39) Sun, Y. S.; Chung, T. M.; Li, Y. J.; Ho, R. M.; Ko, B. T.; Jeng, U. S. *Macromolecules* **2007**, *40*, 6778–6781.
(40) Nojima, S.; Kato, K.; Yamamoto, S.; Ashida, T. *Macromolecules* **1992**, *25*, 2237–2242.
(41) Nojima, S.; Tanaka, H.; Rohadi, A.; Sasaki, S. *Polymer* **1998**, *39*, 1727–1734.
(42) Nojima, S.; Akutsu, Y.; Akaba, M.; Tanimoto, S. *Polymer* **2005**, *46*, 4060–4067.
(43) Albuerne, J.; Márquez, L.; Müller, A. J.; Raquez, J. M.; Degée, P.; Dubois, P.; Castelletto, V.; Hamley, I. W. *Macromolecules* **2003**, *36*, 1633–1644.
(44) Douzinas, K. C.; Cohen, R. E.; Halasa, A. F. *Macromolecules* **1991**, *24*, 4457–4459.
(45) Bittiger, H.; Marchessault, R. H.; Niegisch, W. D. *Acta Crystallogr.* **1970**, *B26*, 1923–1927.
(46) Chen, H. L.; Lin, S. Y.; Huang, Y. Y.; Chiu, F. C.; Liou, W.; Lin, J. S. *Macromolecules* **2002**, *35*, 9434–9440.
(47) Hashimot, T.; Nagatosh, K.; Todo, A.; Hasegawa, H.; Kawai, H. *Macromolecules* **1974**, *7*, 364–373.
(48) Matsushita, Y.; Mori, K.; Saguchi, R.; Nakao, Y.; Noda, I.; Nagasawa, M. *Macromolecules* **1990**, *23*, 4313–4316.
(49) Matsushita, Y.; Mori, K.; Mogi, Y.; Saguchi, R.; Noda, I.; Nagasawa, M.; Chang, T.; Glinka, C. J.; Han, C. C. *Macromolecules* **1990**, *23*, 4317–4321.
(50) Wunderlich, B., *Macromolecular Physics, Crystal Nucleation, Growth, Annealing*. Academic Press: New York, 1976; Vol. *II*.

MA800517K